NASA TECHNICAL NOTE

NASA TN D-2280

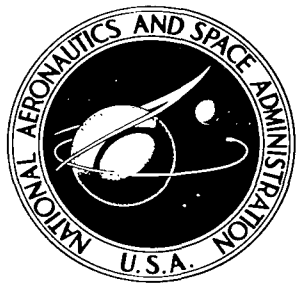

NASA TN D-2280

EXPERIMENTAL LOCAL HEAT-TRANSFER AND AVERAGE FRICTION DATA FOR HYDROGEN AND HELIUM FLOWING IN A TUBE AT SURFACE TEMPERATURES UP TO 5600° R

by Maynard F. Taylor

Lewis Research Center
Cleveland, Ohio

NATIONAL AERONAUTICS AND SPACE ADMINISTRATION • WASHINGTON, D. C. • APRIL 1964

EXPERIMENTAL LOCAL HEAT-TRANSFER AND AVERAGE FRICTION DATA FOR HYDROGEN AND HELIUM FLOWING IN A TUBE AT SURFACE TEMPERATURES UP TO 5600° R

By Maynard F. Taylor

Lewis Research Center
Cleveland, Ohio

NATIONAL AERONAUTICS AND SPACE ADMINISTRATION

For sale by the Office of Technical Services, Department of Commerce,
Washington, D.C. 20230 -- Price $1.00

EXPERIMENTAL LOCAL HEAT-TRANSFER AND AVERAGE FRICTION DATA FOR HYDROGEN AND HELIUM FLOWING IN A TUBE AT SURFACE TEMPERATURES UP TO 5600° R

by Maynard F. Taylor

Lewis Research Center

SUMMARY

Local values of heat-transfer coefficients and average friction coefficients were measured experimentally for helium and hydrogen gases flowing through an electrically heated tungsten tube with a length-to-diameter ratio of 77 for the following range of conditions: local surface temperatures up to 5600° R, local Reynolds number from 7600 to 39,500, local ratios of surface to bulk gas temperature up to 5.6, and heat flux up to 1,700,000 Btu per hour per square foot.

A comparison of local heat-transfer coefficients for helium and hydrogen gases is made for several types of wall temperature distributions in order to determine whether data can be correlated by a Dittus-Boelter type equation.

Wall temperature distributions for hydrogen are compared with one for helium with the result that any dissociation of hydrogen at the tube wall for wall temperatures up to 5200° R has less effect on the wall temperature distribution than does the ratio of surface to bulk gas temperature.

INTRODUCTION

Nuclear reactors, such as those proposed for use in rockets using hydrogen as a propellant, involve heat transfer with large variations in the thermodynamic and transport properties of the gas. These variations can be due to dissociation of the fluid or to large differences between surface and bulk gas temperatures or both. The ratio of surface to gas temperature can be as large as 25 at the inlet of a nuclear reactor if the surface temperature is 5000° R and the inlet gas temperature is 200° R. Some degree of dissociation will occur in the fluid adjacent to the fueled surface through most of the reactor and will occur in the bulk hydrogen at the reactor outlet. The effect of the large variations in the transport properties on the heat-transfer characteris-

tics of hydrogen is very important in the design considerations for nuclear-rocket powered space vehicles.

Considerable experimental data showing the effect of surface to fluid temperature ratio on the heat-transfer coefficient for air are presented in reference 1. A number of other investigations extending over the range of wall temperature, pressure, and ratio of surface to bulk temperature that include helium, hydrogen, and nitrogen have been made and are presented in references 2 to 6. The conditions for which data were obtained in references 1 to 6 and in the present investigation are shown in table I. The present investigation

TABLE I. - EXPERIMENTAL CONDITIONS FOR REFERENCES

Reference	Tube length-to-diameter ratio	Maximum surface to bulk gas temperature ratio	Maximum local surface temperature, ^{o}R	Maximum average surface temperature, ^{o}R	Inlet pressure, $\frac{lb}{sq\ in.}$ abs	Heat-transfer fluid	Types of heat-transfer coefficients measured
1	30 to 120	3.5	----	3050	----------	Air	Average
2	389	1.39	5040	3900	500 to 1500	Helium	Local and average
3	60 and 92	3.9	5900	4533	40	Helium	Local and average
4	20.9 to 42.6	11.09	----	2240	250	Helium and hydrogen	Local
5	250	4.5	2300	----	250 to 1000	Helium and hydrogen	Local
(a)	23.2	4.52	4600	----	110 to 850	Helium and hydrogen	Average
6	127	2.08	1915	----	----------	Nitrogen	Local
Present investigation	77	5.6	5600	4749	40 to 100	Helium and hydrogen	Local

[a]Unpublished data from Herbert J. Newman of Los Alamos Scientific Laboratory.

was intended (1) to extend the range of surface to bulk temperature ratio at high surface temperatures and (2) to determine the effect of dissociation at the surface on the wall temperature distribution. The experiment was performed by flowing helium and hydrogen through an electrically heated tube. A ratio of local surface to bulk temperature of 5.6 and wall temperatures as high as

5600° R were attained at inlet pressures varying from 40 to 100 pounds per square inch absolute.

EXPERIMENTAL APPARATUS

Arrangement

A schematic diagram of the arrangement of the test apparatus used in this investigation is shown in figure 1. Either helium or hydrogen from a pressur-

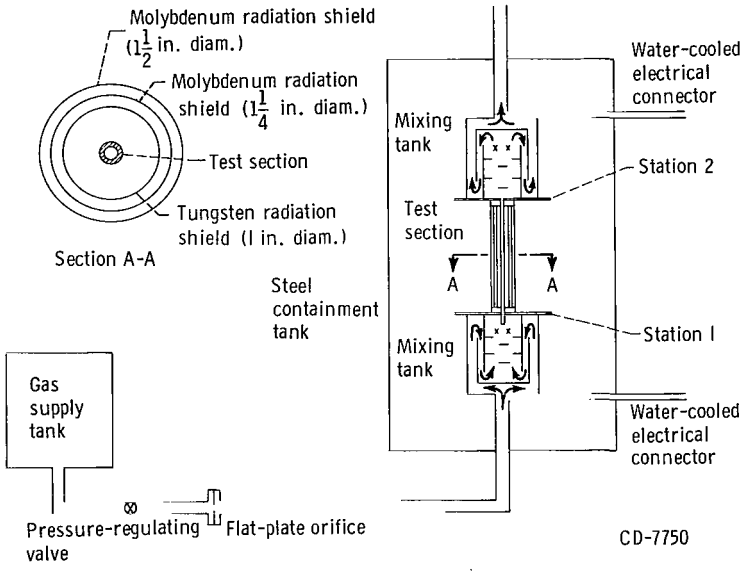

Figure 1. - Schematic diagram of arrangement of test apparatus.

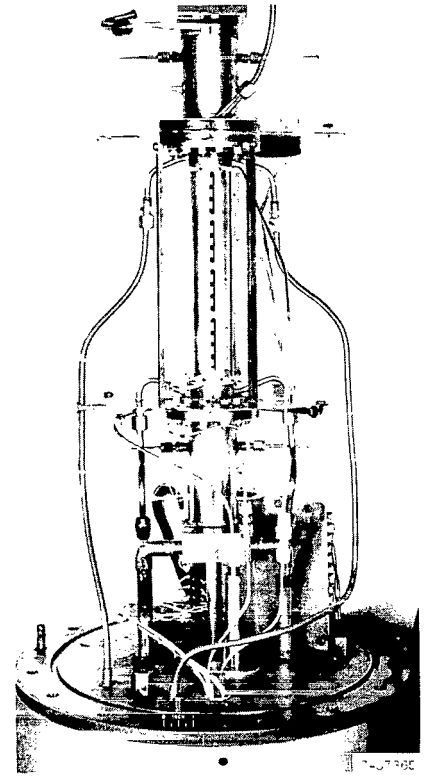

Figure 2. - Experimental apparatus with containment tank removed.

ized tank was passed through the pressure-regulating valve and a flat-plate orifice into a three-pass mixing tank with baffles in the center passage. After mixing, the gas was passed through the electrically heated test section into a second mixing tank and was then exhausted into the atmosphere through a vent stack. The test section was thermally insulated with three concentric radiation shields. The inner shield was made of 0.010-inch-thick tungsten 1 inch in diameter; the middle and outer shields were made of 0.010-inch-thick molybdenum $1\frac{1}{4}$ and $1\frac{1}{2}$ inches in diameter, respectively. Boron nitride spacers were used to hold the shields in position. The mixing tanks and the test-section assembly were housed in a vacuum-tight steel containment tank evacuated to about 25 microns of mercury during test runs. Figure 2 shows the experimental apparatus with the containment tank removed.

Electric power was supplied to the test section through water-cooled copper tubing from a 208-volt 60-cycle supply line through a 100-kilovolt-ampere transformer controlled by a saturable core reactor. The saturable core reactor permitted voltage regulation from approximately 3 to 25 volts. A true root-mean-square electronic voltmeter was used directly to read the potential across the test section. Current was read on an ammeter used with an 800 to 1 step-down current transformer and checked with a calibrated shunt.

Test Sections

The test section used in this investigation was made of tungsten. Since a tungsten tube was not available commercially, it was necessary to fabricate it by disintegrating a hole in a tungsten rod. The hole was lapped to 0.116±0.002-inch inside diameter with a 15- to 20-microinch root mean square finish or better and was concentric with the outside diameter to within a total indicator reading of 0.006 inch. The outside diameter of the tube was then ground to obtain a wall thickness of 0.0625±0.002 inch with a surface finish of 32 microinch root mean square or better. The tungsten tube was joined to water-cooled flanges made of nickel and oxygen-free high conductivity copper with a furnace braze of 82 percent gold and 18 percent nickel at about 1830° F; this temperature is well below the recrystallization temperature of tungsten. The test section was cycled between about 1000° and 5000° R approximately 20 times in the course of the experiment, which totaled about 25 hours of operation at temperatures of 4000° R or higher, and it did not fail. The test section had an entrance length of 14 diameters before the heated section. (All symbols are defined in appendix A.)

Instrumentation

The outside wall temperatures near the entrance and the exit of the test section were measured with 24-gage platinum-platinum-13-percent-rhodium thermocouples spot-welded along the length as shown in figure 3. The temperature of

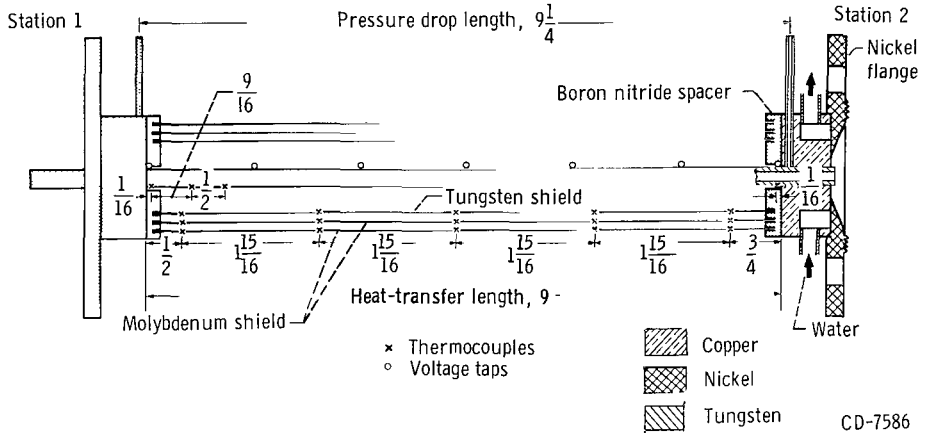

Figure 3. - Schematic diagram of test-section assembly showing thermocouple, voltage tap, and pressure tap locations. (All dimensions in inches.)

most of the test section was measured with a small-target disappearing-filament, optical pyrometer. More information on the technique of temperature measurement used in this investigation can be found in appendix B.

The temperature of the gas was measured at the entrance and the exit of the test section with platinum-platinum-rhodium thermocouples located downstream of the baffles in the two mixing tanks.

The radiation shields were also instrumented with platinum-platinum-rhodium thermocouples as shown in figure 3. Static pressure taps were located in the entrance and the exit flanges of the test section and were read on 0- to 100-pounds-per-square-inch pressure gages having a full-scale accuracy of 1/2 percent. Seven tantalum voltage taps were spot-welded along the test section to measure voltage drop as a function of distance from the entrance; however, only the voltage taps located at the entrance and the exit remained on the test section when it was heated. This arrangement permitted measurement only of the total voltage drop across the test section.

METHOD OF CALCULATION

Hydrogen Properties

The variation of the transport and thermodynamic properties important in calculations of heat-transfer and friction coefficients is shown in figure 4 as a function of temperature for a pressure of 1 atmosphere (data from refs. 7 to 12). The effect of pressure on the properties of hydrogen was not taken into consideration since the pressure was near 1 atmosphere at points in the test section where the temperature was high enough for the pressure effect on dissociation to be appreciable. Figure 4(a) shows the mole fraction of atomic hydrogen x_1 present at any temperature and was taken from references 8 and 9. The thermal conductivity k and the absolute viscosity μ from references 8 to 12 for equilibrium dissociating hydrogen is shown in figures 4(b) and (c). Chemically frozen thermal conductivity, which does not include the chemical reaction term, was taken from reference 9 and is also shown in figure 4(b). The experimental thermal conductivity data shown in figure 4(b) are from reference 7 and are the only data at high temperatures available at present. The values of thermal conductivity used in this investigation are represented by the

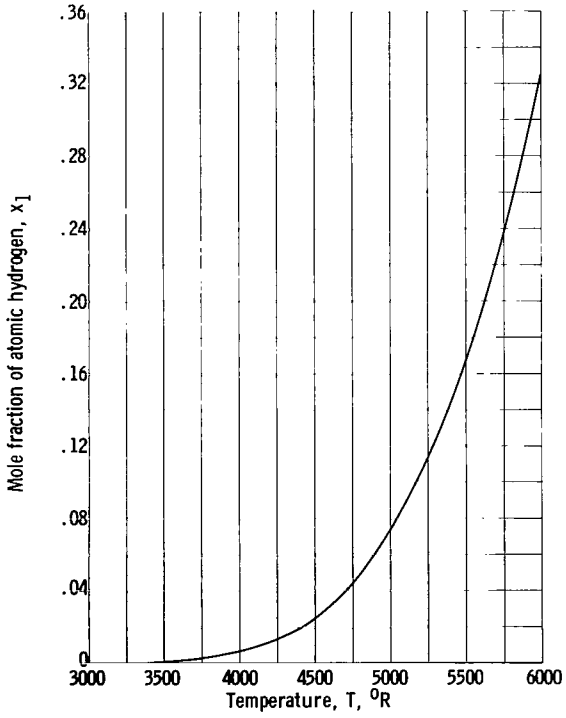

(a) Mole fraction of atomic hydrogen (refs. 8 and 9).

Figure 4. - Variation of hydrogen properties with temperature at 1 atmosphere.

solid line that was calculated by use of the viscosity and thermal conductivity of hydrogen atoms and molecules from table III of reference 11 and the heat of

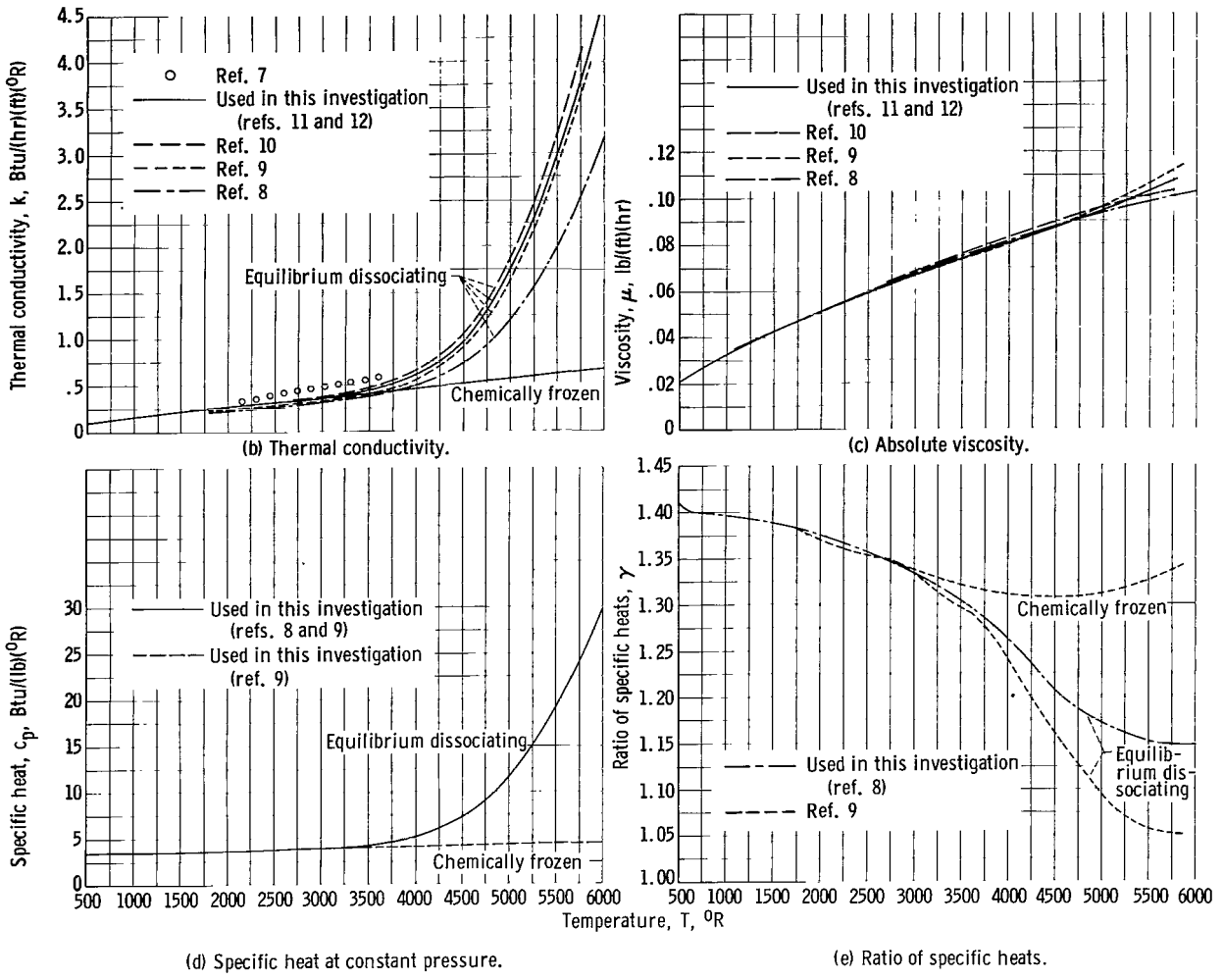

Figure 4. - Concluded. Variation of hydrogen properties with temperature at 1 atmosphere.

dissociation from table XXX of reference 12. The values of specific heat for equilibrium dissociating hydrogen at constant pressure c_p shown in figure 4(d) were taken from references 8 and 9 and are in complete agreement. The chemically frozen specific heat, which does not include the chemical reaction term, was taken from reference 9. The ratio of specific heats γ is taken from references 8 and 9 and is shown in figure 4(e). The two references are in very good agreement at temperatures below 3700° R, a range that more than covers the bulk gas temperatures in this investigation. The gas constant R was taken to be 766.4 foot-pound per pound mass °R.

Helium Properties

The transport properties, thermal conductivity k and absolute viscosity μ for helium used in calculations of this investigation are shown in figure 5

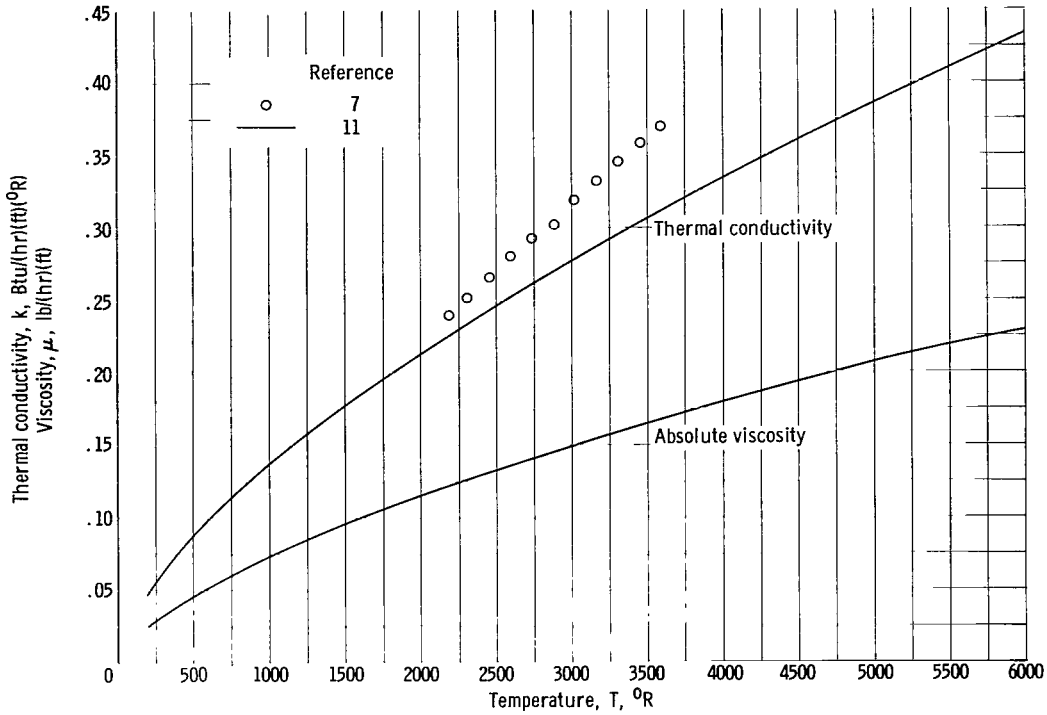

Figure 5. - Variation of thermal conductivity and absolute viscosity of helium with temperature.

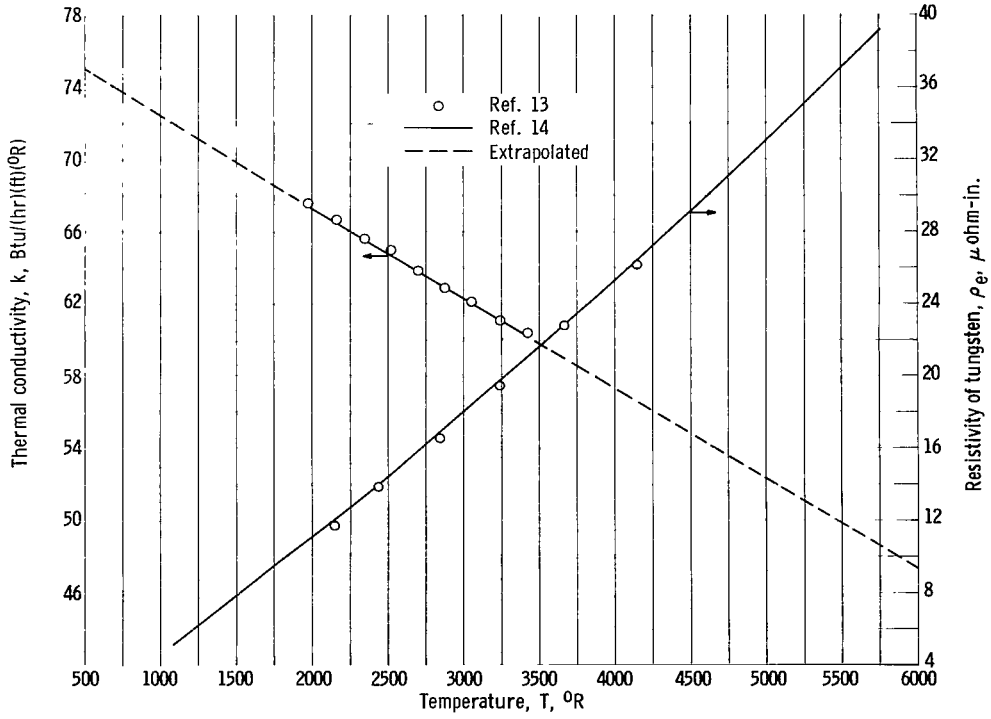

Figure 6. - Variation of thermal conductivity and electrical resistivity of tungsten with temperature.

as a function of temperature. The theoretical values taken from table III of reference 11 are shown along with experimental points from reference 7. The lack of agreement between experiment and theory even for a monatomic gas indicates the great need for more experimental measurements of thermal conductivity of gases at high temperatures. The specific heat at constant pressure c_p was taken to be constant at 1.248 Btu/(lb)($^{\circ}$R), the ratio of specific heats γ to be 1.667, and the gas constant R to be 386 foot-pounds per pound mass $^{\circ}$R.

Physical Properties of Tungsten and Molybdenum

Figure 6 shows both the thermal conductivity k and the electrical resistivity ρ_e of tungsten plotted as a function of temperature. The experimental thermal conductivity data for the temperature range of 2000° to 3600° R were taken from reference 13 and extrapolated, as shown by the dashed line, to cover the range of this investigation. The electrical resistivity was taken from references 13 and 14, which are in agreement to within 3 percent.

The normal total emissivity of both tungsten and molybdenum was taken from reference 14 and is shown in figure 7 as a function of temperature. The spectral emissivity at a wavelength of 0.650 micron was taken from reference 15 and is also shown in figure 7. A discussion of the use of the spectral emissivity is given in appendix B.

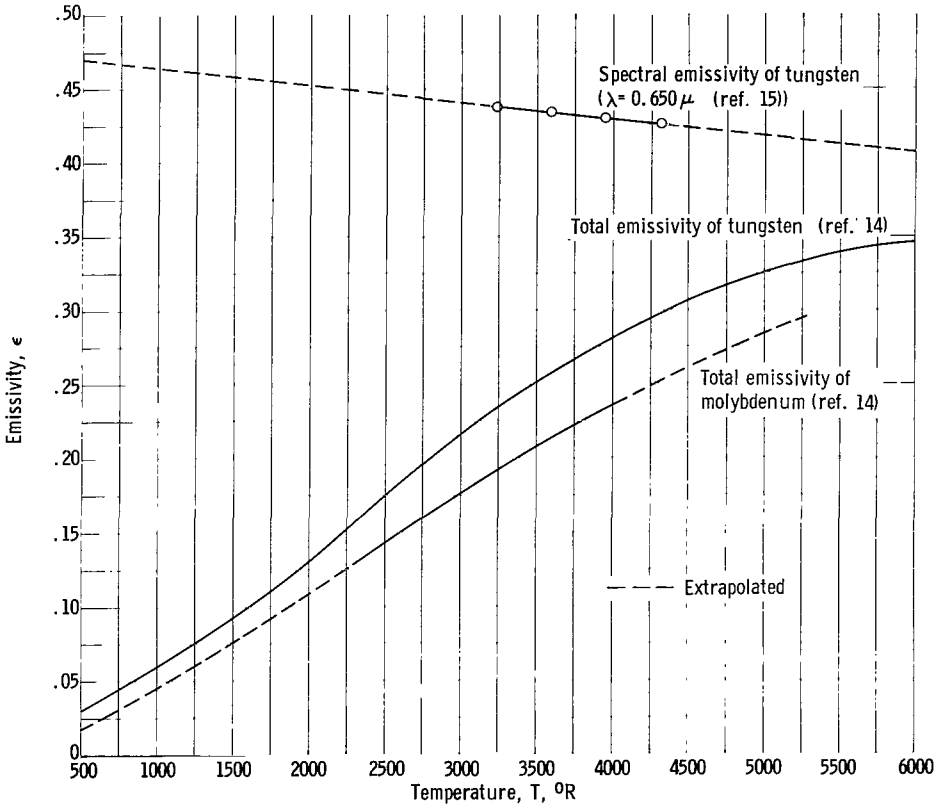

Figure 7. - Variation of emissivity of tungsten and molybdenum with temperature.

Friction Coefficients

Because of the great difficulty in locating static-pressure taps along the tungsten test section, only the overall pressure drops were measured, and, therefore, only average friction coefficients were calculated. The friction pressure drop Δp_{fr} was obtained by subtracting the calculated momentum pressure drop Δp_{mom} from the total measured static-pressure drop Δp across the test section:

$$\Delta p_{fr} = \Delta p - \Delta p_{mom} = \Delta p - \frac{G^2 R}{g}\left(\frac{t_2}{p_2} - \frac{t_1}{p_1}\right) \tag{1}$$

where t_1 and t_2 are the absolute static temperatures at the entrance and the exit of the test section, respectively, and p_1 and p_2 are the static pressures at the entrance and the exit of the test section, respectively. The static temperatures were calculated from measured values of the gas flow, the static pressure, and the total temperature by the following equation:

$$t = -\frac{\gamma g}{(\gamma - 1)R}\left(\frac{p}{G}\right)^2 + \sqrt{\left[\frac{\gamma g}{(\gamma - 1)R}\left(\frac{p}{G}\right)^2\right]^2 + 2T\,\frac{\gamma g}{(\gamma - 1)R}\left(\frac{p}{G}\right)^2} \tag{2}$$

This equation was obtained by combining the perfect gas law, the equation of continuity, and the energy equation. Since the ratio of specific heats γ for hydrogen varies with temperature, the static temperature was calculated twice, once with the specific heat ratio evaluated at the total temperature and once evaluated at the static temperature. The two static temperatures thus calculated varied less than 3 percent of the difference between total and static temperature.

The average friction coefficient was calculated from the relation

$$f = \frac{\Delta p_{fr}}{4\,\frac{L}{D}\,\frac{\rho_{av} V^2}{2g}} = \frac{g \rho_{av}\,\Delta p_{fr}}{2\,\frac{L}{D}\,G^2} \tag{3}$$

where the density ρ_{av} was evaluated from the static pressure and temperature of the gas

$$\rho_{av} = \frac{1}{R}\left(\frac{p_1 + p_2}{t_1 + t_2}\right) \tag{4}$$

Heat-Transfer Coefficients

Only local heat-transfer coefficients were calculated since the heat flux varied by a factor of as much as 7.5 from the entrance to the exit of the test section, as can be seen from the wall temperature distributions shown in fig-

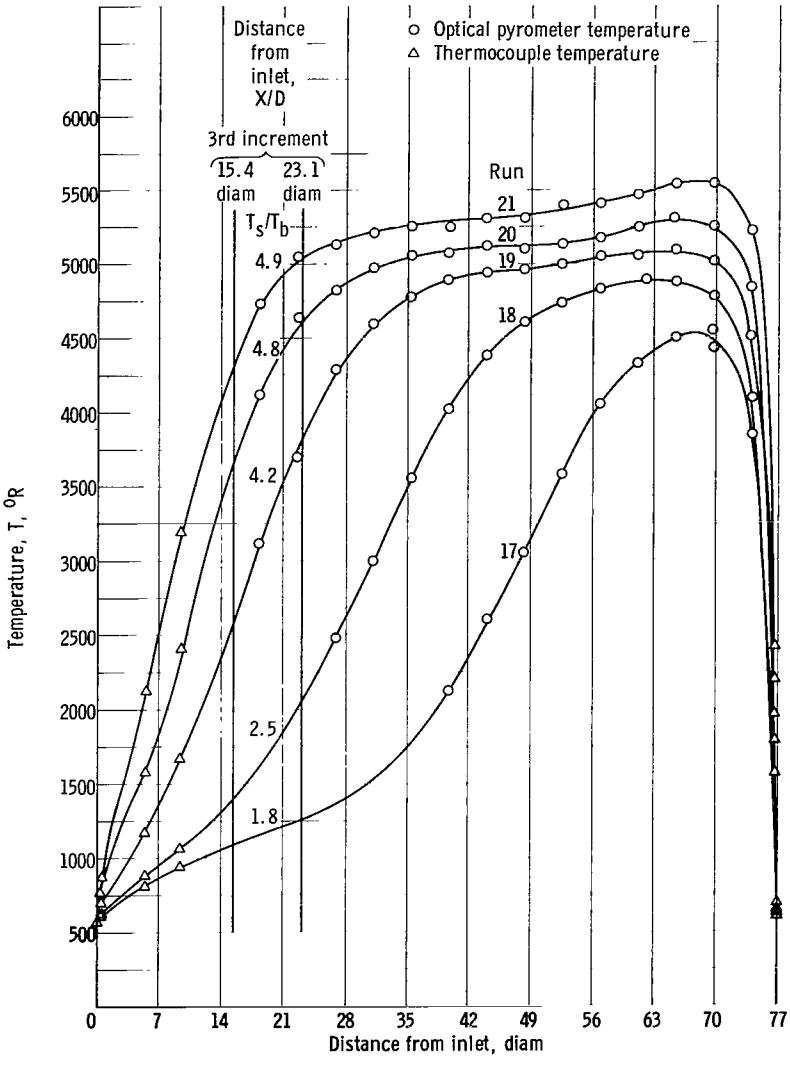

Figure 8. - Comparison of outside wall temperature distributions for increasing amounts of heat input to hydrogen flowing at a constant mass flow rate of 3.8 pounds per hour.

ure 8 and the resistivity of tungsten in figure 6. Local coefficients were approximated by dividing the test section length into 10 equal increments and by evaluating average coefficients for these small increments.

The procedure used to calculate the local heat-transfer coefficient is as follows:

(1) The rate of heat conduction into and away from each increment was calculated by means of the equation

$$Q_c = -k_t A_x \frac{dT}{dL} \qquad (5)$$

where dT/dL is the slope of the axial wall temperature distribution at the end of each increment.

(2) Local radiation heat loss from the test section to the outer radiation shield was calculated by

$$Q_r = \frac{F_A \sigma \left(T_s^4 - T_{r3}^4\right)}{\frac{1}{Fe_{s-r1}A_s} + \frac{1}{Fe_{r1-r2}A_{r1}} + \frac{1}{Fe_{r2-r3}A_{r2}}} \qquad (6)$$

(3) The rate of electrical heat generation in each increment Q_e was calculated by multiplying the square of the current through the test section by the resistance taken from figure 6 for the average wall temperature of the increment.

(4) A heat balance for each increment was set up starting at the entrance

$$Q_e + \left[Q_{c(n)} - Q_{c(n+1)}\right] - Q_r - Q = 0 \qquad (7)$$

It was possible to calculate the rate of heat transfer to the gas Q for each increment from equation (7). The bulk temperature of the gas leaving each increment could be calculated by means of the equation

$$Q = w(c_p)_b(T_{out} - T_{in}) \tag{8}$$

where T_{in} is the bulk temperature of the gas entering the increment and T_{out} is the bulk temperature of the gas leaving the increment. This calculation was repeated for each succeeding increment, and the calculated temperature of the gas leaving the last increment was used as the exit gas temperature. This temperature was used along with the measured exit gas temperature, the gas flow rate, and the physical properties to determine heat-transfer coefficients from the Dittus-Boelter equation. The heat-transfer coefficient was used to calculate the rate of heat transfer to the water-cooled exit flange.

(5) In general, the sum of the local radiation heat losses and the end losses was found to account for more than 80 percent of the difference between the rate of electrical heat input to the test section and the rate of heat transfer to the gas. Each local radiation heat loss and the two end losses were multiplied by the ratio of total heat loss to the sum of local heat losses and the two end losses for adjustment to give an overall heat balance of 100 percent.

(6) A new heat balance was set up by use of the adjusted local heat losses and equation (7), and the rate of heat transfer to the gas Q was calculated. The bulk temperature of the gas leaving each increment was calculated by means of equation (8).

(7) The local bulk temperature and the local surface temperature along with the rate of heat transfer to the gas and the heat-transfer area for the increment were used to calculate the local heat-transfer coefficient

$$h = \frac{Q}{S(T_s - T_b)} \tag{9}$$

The temperature drop through the wall was calculated and found to be very small compared with the difference between surface and bulk temperatures and, therefore, was neglected.

The local Nusselt number was calculated by means of the relation

$$Nu = \frac{hD}{k} \tag{10}$$

RESULTS AND DISCUSSION

Axial Wall Temperature Distributions

Five representative axial outside wall temperature distributions are plotted as a function of the distance from the inlet for a tungsten tube with a total length to diameter ratio of 77 (fig. 8). Thermocouple and optical pyrometer measurements for each run are also shown in the figure. Experimental data for all runs are summarized in table II (see pp. 27 to 32). The wall tempera-

ture distributions shown in figure 8 are for hydrogen but are also typical of those obtained for helium. For runs 17 to 21, the mass flow rate was kept nearly constant, while the power input was increased to higher levels. The relatively large increase in wall temperature in the entrance half of the tube, as power input is increased, is a result of two factors. First, the ratio of surface to bulk fluid temperature is increased, which is accompanied by a decrease in heat-transfer coefficient that further increases the surface temperature. Second, the effect of increasing the ratio of surface to bulk fluid temperature is magnified by the increased electrical resistivity of tungsten at higher temperatures. The large axial temperature gradients at the entrance and the exit of the test section are the result of conduction losses to the connecting flanges, the mixing tanks, and the electrical connectors.

It was thought that the best way of determining the effect of dissociation at the wall was to compare the wall temperature distribution for hydrogen with the wall temperature distribution for helium under the same conditions. It can be shown that when the product of flow rate w and specific heat c_p of hydrogen is equal to that for helium and the heat input to hydrogen is equal to the heat input to helium, then the heat-transfer coefficient and the wall temperature distributions for helium and hydrogen should be essentially the same if dissociation does not affect the heat-transfer coefficient. The first two conditions were approached quite closely by helium run 15 and hydrogen run 19. The heat input was 2 percent less and the product of flow rate and specific heat was 3 percent less for the hydrogen run than for the helium run, while the heat-transfer coefficients were 10 to 15 percent higher for hydrogen than for helium. The wall temperature distribution for helium run 15 and hydrogen runs 19 and 20 are shown in figure 9 as a function of

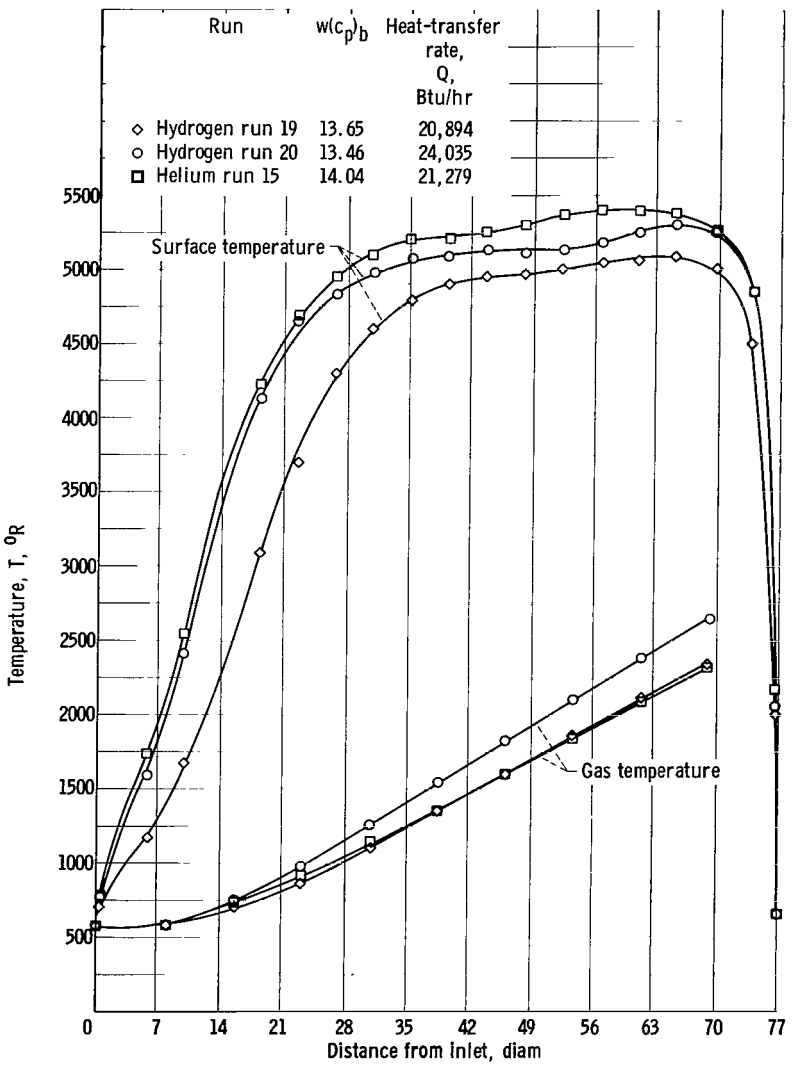

Figure 9. - Comparison of outside wall temperature distributions and gas temperatures of hydrogen and helium for mass flow rate ratio inversely proportional to ratio of specific heats, $w_{He}/w_{H_2} = (c_p)_{H_2}/(c_p)_{He}$.

distance from the inlet. It can be seen in figure 9 that the largest difference between the wall temperatures of runs 15 and 19 occurs where the wall temperature is too low for dissociation to occur. It appears that any dissociation at the tube wall has less effect on the wall temperature distribution than does the ratio of surface to bulk gas temperatures. The wall temperature distribution for hydrogen run 20 is also shown in figure 9 and appears to be quite similar to helium run 15. For this run, the heat input to the hydrogen is 12 percent greater than the heat input to the helium, and the product of flow rate and specific heat for hydrogen was about 4 percent lower than that for helium, which results in hydrogen heat-transfer coefficients 25 to 30 percent higher than those for helium. The heat-transfer parameters for the helium run and the two hydrogen runs are shown in figures 10(a) and (b). The parameters

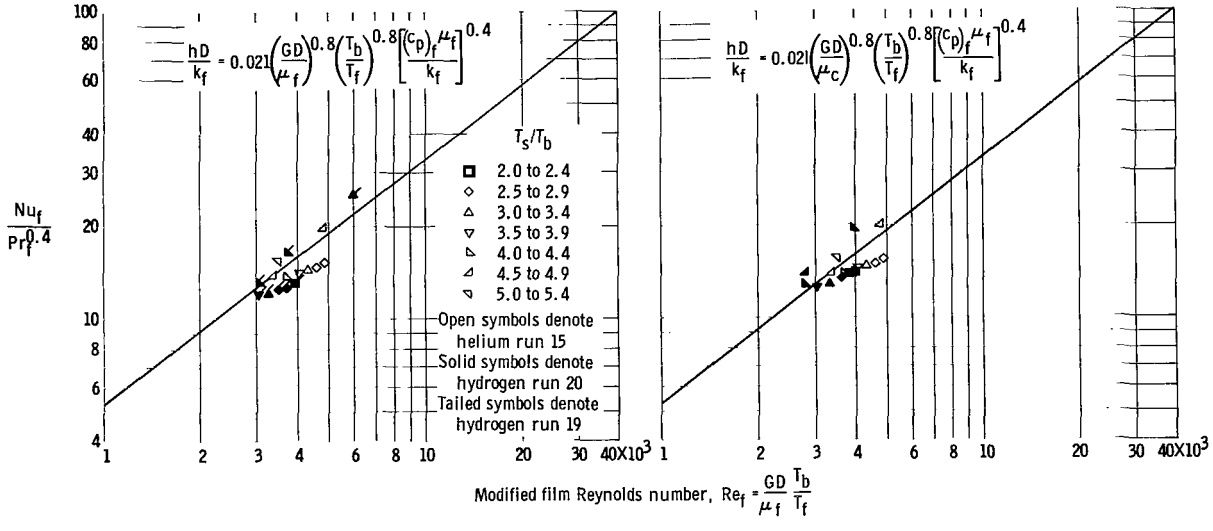

(a) Runs 15 and 19. (b) Runs 15 and 20.

Figure 10. - Comparison of local heat-transfer coefficients for helium and hydrogen.

for the hydrogen runs (particularly run 19) compare quite closely with those for helium.

Friction Coefficients

Only average friction coefficients were measured in this investigation. The friction coefficients for helium and hydrogen both with and without heat addition are shown in figures 11(a) and (b), respectively. The line representing the Kármán-Nikuradse relation between friction coefficient and Reynolds number for turbulent flow given by

$$\frac{1}{\sqrt{8\,\frac{f}{2}}} = 2 \log Re\left(\sqrt{8\,\frac{f}{2}}\right) - 0.8 \qquad (11)$$

and the laminar flow line given by

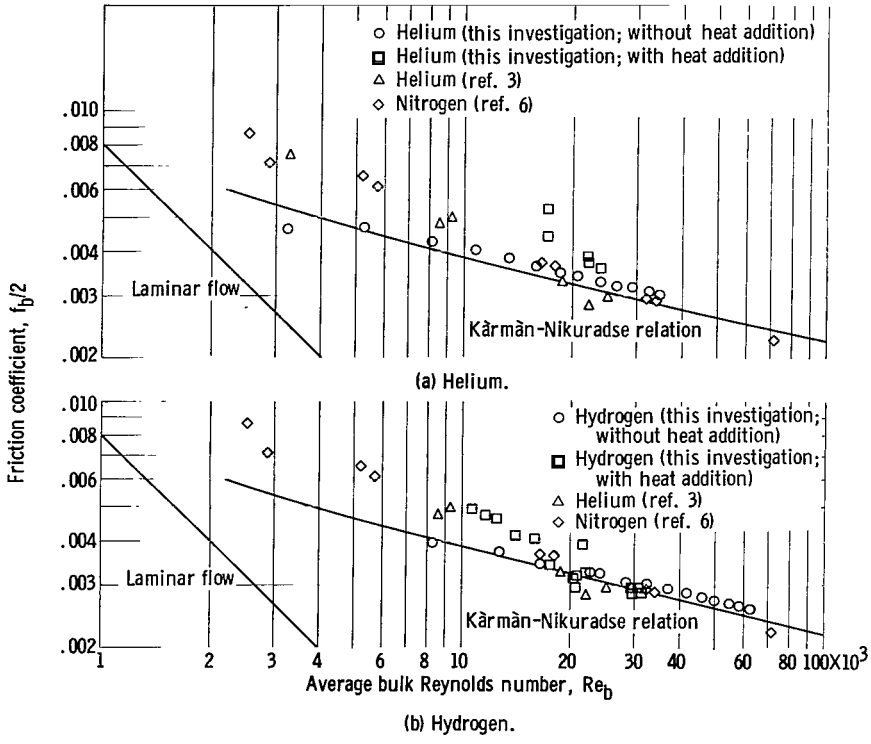

Figure 11. - Correlation of average friction coefficients. Viscosity and density evaluated at bulk temperature. Kàrmàn-Nikuradse relation, $1/\sqrt{8f_b/2} = 2\log(Re_b\sqrt{8f_b/2}) - 0.8$; laminar flow, $f_b/2 = 8/Re_b$.

$$\frac{f}{2} = \frac{8}{Re} \tag{12}$$

are included in figure 11 for comparison.

As would be expected, the hydrogen and helium runs with no heat addition are in good agreement with the Kármán-Nikuradse relation. The hydrogen runs with heat addition are in agreement with the predicted line above a Reynolds number of 20,000 and in agreement with the data of references 3 and 6, which fall above the Kármán-Nikuradse line below a Reynolds number of 20,000. The few runs using helium fall somewhat higher than either the predicted line or the data of references 3 and 6.

Heat-Transfer Coefficients

In the present investigation, only local heat-transfer coefficients were calculated. The results of reference 3 for helium indicate that local heat-transfer coefficients can be correlated by use of a modified Reynolds number, evaluation of the physical properties and the density at either the film or the surface reference temperature, and use of an appropriate constant, as shown in the following equations:

$$\frac{hD}{k_f} = 0.021\left(\frac{GD}{\mu_f}\right)^{0.8}\left(\frac{T_b}{T_f}\right)^{0.8}\left[\frac{(c_p)_f\mu_f}{k_f}\right]^{0.4} \tag{13}$$

$$\frac{hD}{k_s} = 0.0265\left(\frac{GD}{\mu_s}\right)^{0.8}\left(\frac{T_b}{T_s}\right)^{0.8}\left[\frac{(c_p)_s\mu_s}{k_s}\right]^{0.4} \qquad (14)$$

As stated in reference 3, evaluating the fluid properties at the surface temperature results in a slightly better correlation than that given by evaluating the properties at the film temperature, although the constant is higher than that given in the literature. All the helium data of the present investigation are shown in figure 12(a) with the fluid properties evaluated at the film temperature and in figure 12(b) with the properties evaluated at the surface temperature. There is considerable spread in the data when each reference

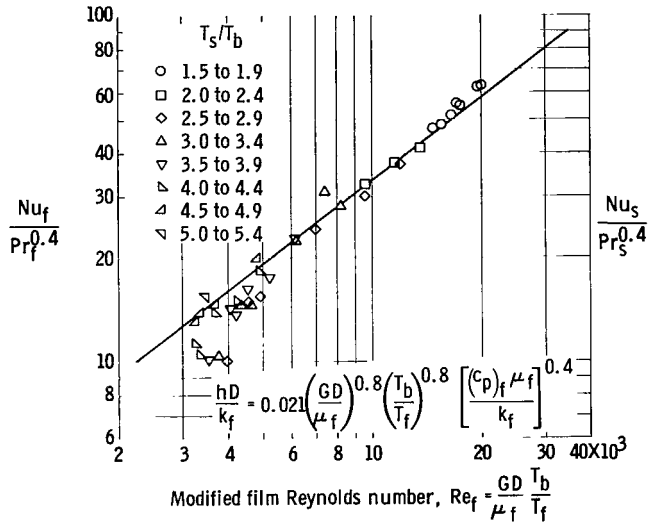

(a) Fluid properties evaluated at film temperature; runs 12 to 16.

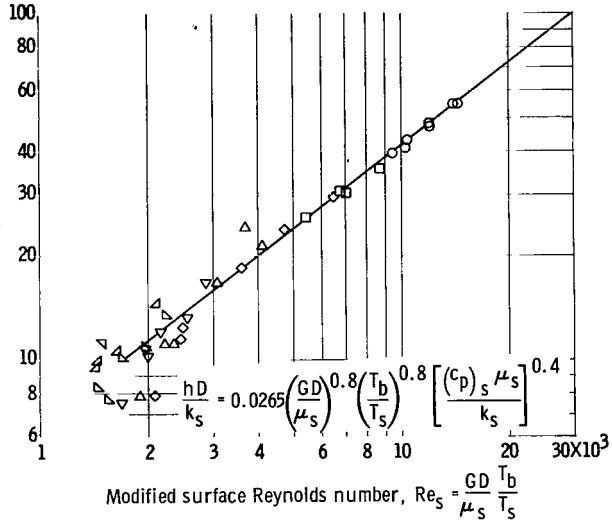

(b) Fluid properties evaluated at surface temperature; runs 12 to 16.

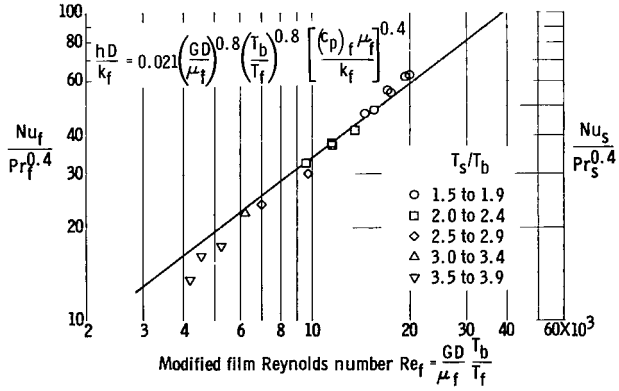

(c) Fluid properties evaluated at film temperature; runs 12 and 13.

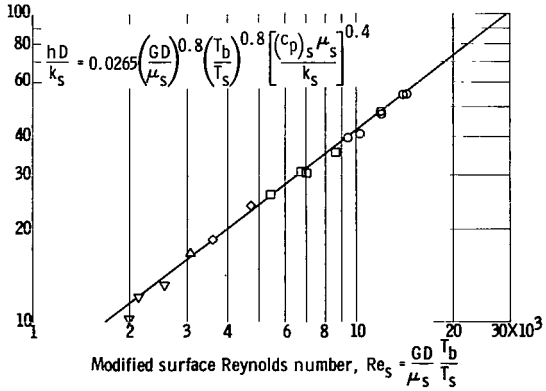

(d) Fluid properties evaluated at surface temperature; runs 12 and 13.

Figure 12. - Correlation of local heat-transfer coefficients for helium.

temperature is used. This is not a random scatter as it appears but has definite trends that depend on the shape of the wall temperature distribution and the power input. If the wall temperature distribution is similar in shape to run 17, shown in figure 8, the data correlate, as shown in figures 12(c) and (d). It can be seen that the data correlate better if the fluid properties are evaluated at the surface temperature. If the wall temperature distribution resembles that of runs 18 to 21, neither reference temperature correlates the data satisfactorily (see figs. 12(e) and (f)). It is not apparent from figures 12(e) and (f), but these data do not fall with random scatter either, but rather with a definite trend from run to run. To show the trend in data with the fluid properties evaluated at the various reference temperatures, $Nu/Pr^{0.4}$ is plotted as a function of modified Reynolds number in figure 13 for runs 12 and 15, which are typical of two shapes of wall temperature distributions. The fluid properties are evaluated at bulk, film, and surface temperatures. The difference in trends between runs 12 and 15 can easily be seen.

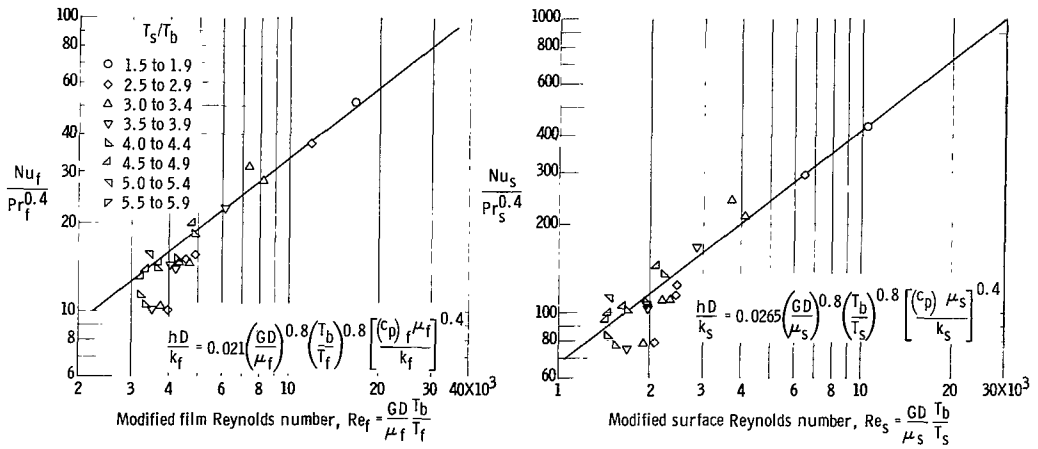

(e) Fluid properties evaluated at film temperature; runs 14 to 16.

(f) Fluid properties evaluated at surface temperature; runs 14 to 16.

Figure 12. - Concluded. Correlation of local heat-transfer coefficients for helium.

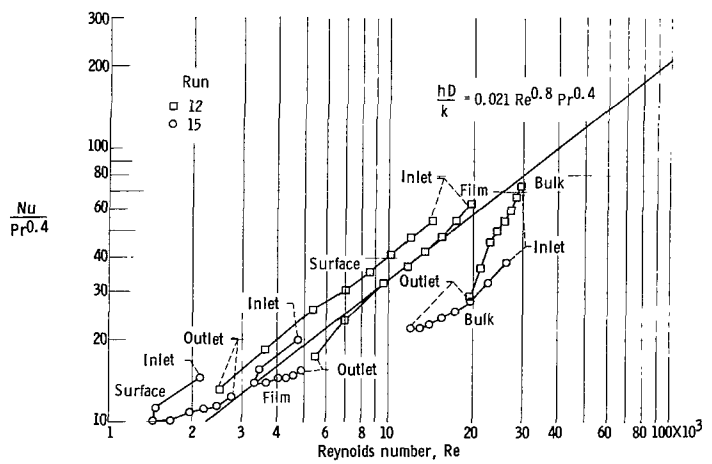

Figure 13. - Comparison of effect of using fluid properties evaluated at bulk, film, and surface temperatures on correlation of local heat-transfer coefficients for two helium runs.

Figure 14(a) shows all the hydrogen data with the fluid properties evaluated only at the film temperature. The film temperature was not high enough for dissociation to occur. Again the data can be separated according to the criterion of wall temperature distribution shape. The runs having the shape of run 17 of figure 8 are plotted in figures 14(b) and (c) with the fluid properties evaluated at the film and the surface temperatures, respectively. For these runs, the surface temperature is below the temperature at which dissociation has an appreciable effect on the fluid properties. As with helium, the hydrogen data correlate best when the fluid properties are evaluated at the surface temperature. The constant 0.0265 for helium has been replaced by 0.0245. Runs with wall temperature distribution of the shapes of runs 18 to 21 are shown in figure 14(d) with the fluid properties evaluated at the film temperature. As with helium, this type of wall temperature distribution yields data that do not correlate very well by conventional methods. The effects of reference temperature and the use of both equilibrium dissociating and chemically frozen transport and thermodynamic properties are shown in figure 15. The reason for a low value of $Nu/Pr^{0.4}$ for equilibrium dissociating proper-

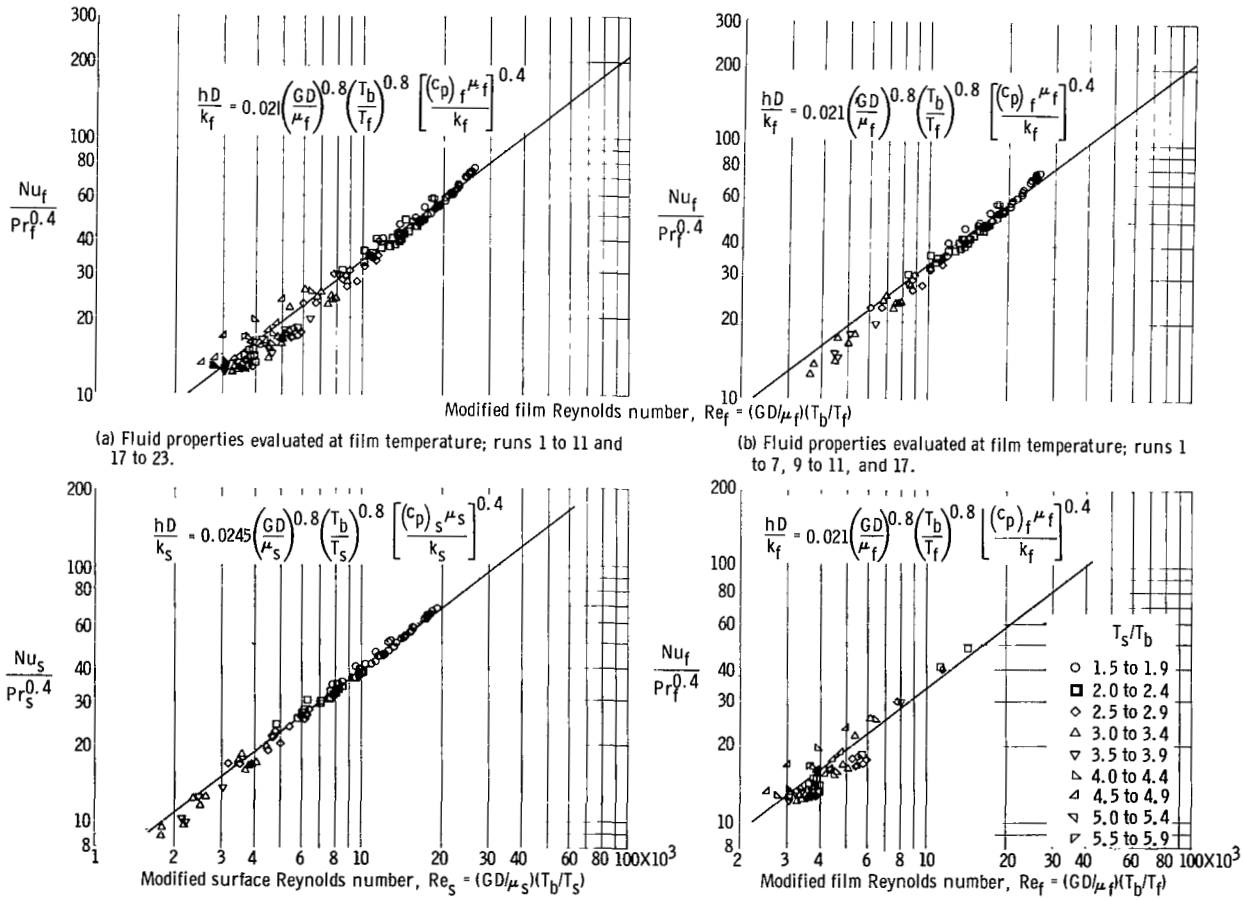

(a) Fluid properties evaluated at film temperature; runs 1 to 11 and 17 to 23.

(b) Fluid properties evaluated at film temperature; runs 1 to 7, 9 to 11, and 17.

(c) Fluid properties evaluated at surface temperature; chemically frozen thermal conductivity and specific heat; runs 1 to 7, 9 to 11, and 17.

(d) Fluid properties evaluated at film temperature; runs 8 and 18 to 23.

Figure 14. - Correlation of local heat-transfer coefficients for hydrogen.

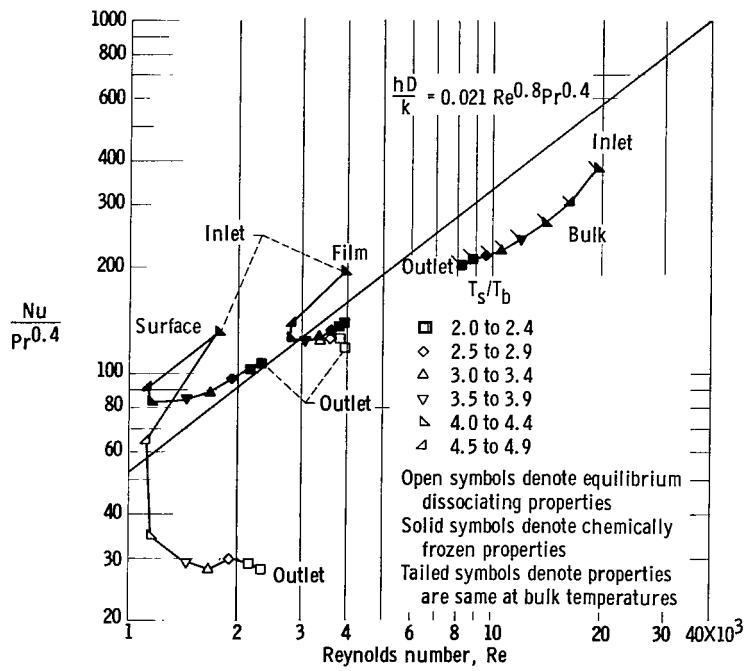

Figure 15. - Comparison of effect of using fluid properties evaluated at bulk, film, and surface temperatures on correlation of local heat-transfer coefficients with equilibrium dissociating and chemically frozen transport and thermodynamic properties for hydrogen run 20.

ties is the large increase in the thermal conductivity with increasing temperature.

The data of this investigation indicate that little difference is made by the use of film or surface reference temperature to predict heat-transfer coefficients (fig. 15). It is important, however, that the chemically frozen transport and thermodynamic properties be used rather than the equilibrium dissociating properties. The result of using chemically frozen and equilibrium dissociating properties can be seen in figure 15. It is obvious from this figure that a better method of correlation is needed.

Data have been obtained in this investigation that agree with previous correlations in the literature using modified Reynolds number and properties evaluated at film or surface temperature; however, some data obtained with large axial gradients in heat flux and surface temperature near the entrance of the test section introduce deviations of ±30 percent from the correlation.

SUMMARY OF RESULTS

The following results were obtained in an investigation of heat transfer and pressure drop for helium and hydrogen at pressures of 40 to 100 pounds per square inch flowing through a tungsten tube at surface temperatures up to 5600° R:

1. Any dissociation at the tube surface has less effect on the wall temperature distribution than does the ratio of surface to bulk gas temperatures at surface temperatures up to 5200° R.

2. Most local heat-transfer data agree to within ±10 percent when correlated by using the Dittus-Boelter equation and chemically frozen viscosity, thermal conductivity, and specific heat. These physical properties and density were evaluated at either the film or the surface temperature. Some data obtained with large axial gradients in heat flux and surface temperature near the test section entrance introduce deviations of ±30 percent from the correlation equation.

3. Friction coefficients without heat addition are in good agreement with

the Kármán-Nikuradse relation. Friction coefficients with heat addition are in poor agreement with the Kármán-Nikuradse line below a Reynolds number of about 20,000 but are in good agreement with the data of other investigators.

Lewis Research Center
National Aeronautics and Space Administration
Cleveland, Ohio, January 31, 1964

APPENDIX A

SYMBOLS

A_{r1} surface area of inner radiation shield, sq ft

A_{r2} surface area of middle radiation shield, sq ft

A_{r3} surface area of outer radiation shield, sq ft

A_s outside surface area of test section, sq ft

A_x cross-sectional area of tube wall, sq ft

C_2 radiation constant, 25,891 (micron)($^\circ$R), appendix B

c_p specific heat of the gas at constant pressure, Btu/(lb)($^\circ$R)

D inside diameter of test section, ft

ΔE potential drop, v

F_A configuration factor for radiation

Fe_{s-r1} factor to allow for the departure of the test section and inner radiation shield surfaces from complete blackness, $\dfrac{1}{\frac{1}{\epsilon_s} + \frac{A_s}{A_{r1}}\left(\frac{1}{\epsilon_{r1}} - 1\right)}$

Fe_{r1-r2} factor to allow for the departure of inner and middle radiation shields from complete blackness, $\dfrac{1}{\frac{1}{\epsilon_{r1}} + \frac{A_{r1}}{A_{r2}}\left(\frac{1}{\epsilon_{r2}} - 1\right)}$

Fe_{r2-r3} factor to allow for the departure of middle and outer radiation shields from complete blackness, $\dfrac{1}{\frac{1}{\epsilon_{r2}} + \frac{A_{r2}}{A_{r3}}\left(\frac{1}{\epsilon_{r3}} - 1\right)}$

f average friction coefficient

G mass flow per unit cross-sectional area, lb/(hr)(sq ft)

g acceleration due to gravity, 4.17×10^8 ft/hr^2

h local heat-transfer coefficient, Btu/(hr)(sq ft)($^\circ$R)

I current, amp

k	thermal conductivity of gas, Btu/(hr)(ft)(^{o}R)
k_t	thermal conductivity of test section material, Btu/(hr)(ft)(^{o}R)
L	heat-transfer length of test section, ft
Nu	Nusselt number based on local heat-transfer coefficient, hD/k
Pr	Prandtl number, $c_p\mu/k$
p	absolute static pressure, lb/sq ft
Δp	overall static-pressure drop across test section, lb/sq ft
Δp_{fr}	friction static-pressure drop across test section, lb/sq ft
Δp_{mom}	momentum static-pressure drop across test section, lb/sq ft
Q	rate of heat transfer to gas, Btu/hr
Q_c	rate of heat conduction through tube wall in axial direction, Btu/hr
Q_e	rate of electrical heat input to increment, Btu/hr
Q_r	rate of heat loss from test section through radiation shields, Btu/hr
R	gas constant, ft-lb/(lb_{mass})(^{o}R)
Re	Reynolds number, GD/μ
r	resistance of test section, ohms
S	heat-transfer area of test section, sq ft
T	total or stagnation temperature, ^{o}R
T_b	average bulk temperature for an increment, $(T_n + T_{n+1})/2$, ^{o}R
T_{bb}	blackbody temperature, ^{o}R
T_{br}	brightness temperature (apparent temperature of nonblackbody), ^{o}R
T_f	average film temperature, $(T_s + T_b)/2$, ^{o}R
T_{in}	bulk temperature of the gas entering an increment, ^{o}R
T_{out}	bulk temperature of the gas leaving an increment, ^{o}R
T_{r3}	temperature of an increment of the outside radiation shield, ^{o}R
T_s	average surface temperature of an increment, ^{o}R

T_τ apparent brightness temperature (apparent temperature of nonblackbody with view window interposed), $^\circ R$

t static temperature, $^\circ R$

V bulk velocity of gas, ft/hr

w gas flow, lb/hr

X distance from entrance of test section, ft

γ ratio of specific heats of gas

ϵ_{r1} normal total emissivity of inner radiation shield

ϵ_{r2} normal total emissivity of middle radiation shield

ϵ_{r3} normal total emissivity of outer radiation shield

ϵ_s normal total emissivity of test section

ϵ_λ spectral emissivity

λ wavelength (effective wavelength of small-target optical pyrometer filter), microns

μ absolute viscosity of gas, lb/(hr)(ft)

ρ density of gas, lb/cu ft

ρ_{av} average density of gas, $(p_1 + p_2)/R(t_1 + t_2)$, lb/cu ft

ρ_e resistivity of tungsten, μohm-in.

σ Stefan-Boltzmann constant, 0.173×10^{-8} Btu/(hr)(ft)^2($^\circ R$)^4

τ_λ spectral transmissivity of view windows

Subscripts:

b bulk (when applied to properties, indicates evaluation at average bulk temperature T_b)

f film (when applied to properties, indicates evaluation at average film temperature T_f)

s surface (when applied to properties, indicates evaluation at average surface temperature T_s)

1 test section entrance

2 test section exit

APPENDIX B

METHOD OF OPTICAL PYROMETER

As mentioned in the text, the temperature of most of the test section was measured with a small-target disappearing-filament optical pyrometer. It is shown in the appendix of reference 3 that from Wien's formula for blackbody radiation a relation between the true temperature of the test section and the brightness temperature indicated by the pyrometer can be obtained, and the relation follows:

$$T_{bb} = \frac{\frac{C_2}{\lambda}}{\ln(\epsilon_\lambda \tau_\lambda) + \frac{C_2}{\lambda T_\tau}} \tag{B1}$$

where T_{bb} is the true blackbody temperature of the test section, T_τ is the measured temperature, ϵ_λ is the emissivity of the test section, τ_λ is the transmissivity of any view windows interposed, λ is the wavelength of the optical-pyrometer filter (0.650 micron), and C_2 is the radiation constant (25,891 (micron)($^\circ$R)).

The transmissivity of any view windows can be determined very easily by measuring the temperature of a calibration lamp both with and without the windows and by inserting the values obtained in the equation

$$\ln \tau_\lambda = \frac{C_2}{\lambda}\left(\frac{1}{T_{br}} - \frac{1}{T_\tau}\right) \tag{B2}$$

where T_{br} and T_τ are the temperature measured without and with the view window interposed, respectively. The transmissivities of the 3/8-inch quartz view window on the containment tank and the $1\frac{1}{4}$-inch upright optical glass safety window were measured experimentally and found to be 0.928 and 0.883, respectively.

The spectral emissivity of tungsten given in reference 16 was used along with the transmissivity of the windows to calculate the wall temperatures of the test section from equation (B1). The wall temperatures were plotted as a function of distance from the test section entrance and then were integrated to determine the average wall temperature. The average wall temperature was also found by calculating the resistance of the test section from the potential drop across it and the current. The resistivity of the test section can be calculated from the equation

$$\rho_e = \frac{rA_x}{L} \tag{B3}$$

From the curve of resistivity as a function of temperature in figure 6, the average temperature of the test section can be determined from the resistivity value. The average wall temperatures determined by the two methods disagreed less than 5 percent for most runs.

REFERENCES

1. Humble, Leroy V., Lowdermilk, Warren H., and Desmon, Leland G.: Measurements of Average Heat-Transfer and Friction Coefficients for Subsonic Flow of Air in Smooth Tubes at High Surface and Fluid Temperatures. NACA Rept. 1020, 1951.

2. Durham, F. P., Neal, R. C., and Newman, H. J.: High Temperature Heat Transfer to a Gas Flowing in Heat Generating Tubes with High Heat Flux. TID-7529, pt. 1, book 2, Reactor Heat Transfer Conf., Nov. 1957, pp. 502-514.

3. Taylor, Maynard F., and Kirchgessner, Thomas A.: Measurements of Heat Transfer and Friction Coefficients for Helium Flowing in a Tube at Surface Temperatures up to 5900° R. NASA TN D-133, 1959. (See also ARS Jour., vol. 30, 1960, pp. 830-832.)

4. Wolf, H., and McCarthy, J. R.: Heat Transfer to Hydrogen and Helium with Wall to Fluid Temperatures Ratios to 11.09. Presented at the AIChE Annual Meeting, Washington (D.C.), Dec. 4-7, 1960.

5. Weiland, Walter F.: Measurement of Local Heat Transfer Coefficients for Flow of Hydrogen and Helium in a Smooth Tube at High Surface to Fluid Bulk Temperature Ratios. Presented at AIChE Nuclear Engineering Heat Transfer Symposium, Chicago (Ill.), Dec. 1962.

6. Davenport, Monty E., Magee, Patrick M., and Lepert, George: Heat Transfer and Pressure Drop for a Gas at High Temperature. SU 247-2, Nuclear Technology Laboratory, Stanford University, May 1961. (TID-13485.)

7. Blais, Normand C., and Mann, Joseph B.: Thermal Conductivity of Helium and Hydrogen at High Temperatures. Jour. Chem. Phys., vol. 32, no. 5, May 1960, pp. 1459-1465.

8. King, Charles R.: Compilation of Thermodynamic Properties, Transport Properties, and Theoretical Rocket Performance of Gaseous Hydrogen. NASA TN D-275, 1960.

9. Rosner, Daniel E.: Properties of Equilibrium Dissociating Hydrogen for Predicting Convective Heating in Nuclear-Thermal Rockets. Tech. Pub. 27, AeroChem Res. Lab., Inc., 1961.

10. Clifton, David G.: Calculations of the Coefficients of Viscosity, Diffusion, and Thermal Conductivity for Dissociating Hydrogen for a Range of Temperatures and Pressure. Los Alamos Scientific Laboratory Rept. LA-2475, 1960.

11. Svehla, Roger A.: Estimated Viscosities and Thermal Conductivities of Gases at High Temperatures. NASA TR R-132, 1962.

12. Huff, Vearl N., Gordon, Sanford, Morrell, Virginia E.: General Method and Thermodynamic Tables for Computation of Equilibrium Composition and Temperature of Chemical Reactions. NACA Rept. 1037, 1951.

13. Osborn, R. H.: Thermal Conductivities of Tungsten and Molybdenum at Incandescent Temperatures. Jour. Opt. Soc. Am., vol. 31, June 1941, pp. 428-432.

14. Hodgman, Charles D., ed.: Handbook of Chemistry and Physics, forty-third ed., Chem. Rubber Pub. Co., 1961-62.

15. Larrabee, Robert D.: Spectral Emissivity of Tungsten. Jour. Opt. Soc. Am., vol. 49, no. 6, June 1959, pp. 619-625.

TABLE II. - EXPERIMENTAL RESULTS

(a) For complete test section

Run	Heat input, Q_e/S, $\frac{Btu}{(hr)(sq\ ft)}$	Heat transfer, Q/S, $\frac{Btu}{(hr)(sq\ ft)}$	Gas flow, w, $\frac{lb}{hr}$	Entrance pressure, p_1, $\frac{lb}{sq\ ft}$ abs	Exit pressure, p_2, $\frac{lb}{sq\ ft}$ abs	Entrance temperature, $T_{b,1}$, ^oR	Exit temperature, $T_{b,2}$, ^oR	Average bulk temperature, $T_{b,av}$, ^oR	Average surface temperature of test section, $T_{s,av}$, ^oR	Current, I, amp	Potential drop, ΔE, v
					Hydrogen						
1	698,346	586,404	6.91	8,621	3077	568	1135	852	1768	1392	2.9
2	583,848	537,819	6.86	8,355	3056	568	1090	829	1559	1378	2.83
3	830,170	680,248	7.04	9,118	3254	568	1213	891	1954	1420	4.0
4	665,390	568,550	6.59	8,287	2902	563	1138	851	1744	1370	3.05
5	721,898	623,287	6.91	8,834	3082	567	1168	868	1803	1400	3.45
6	755,159	657,314	6.95	8,978	3118	560	1192	876	1836	1412	3.7
7	910,013	755,686	7.02	9,338	3293	568	1288	928	2120	1420	4.0
8	1,843,187	1,409,408	6.15	10,653	3758	570	2076	1323	3950	1400	8.85
9	669,308	507,536	4.99	6,967	2388	562	1242	902	2040	1250	3.6
10	906,704	672,216	5.38	7,708	2745	565	1401	983	2444	1300	4.73
11	1,026,731	756,347	5.22	7,798	2822	567	1531	1052	2731	1292	4.98
					Helium						
12	556,552	407,601	12.08	11,100	3470	572	1193	883	1974	1158	2.88
13	737,614	509,295	11.88	11,772	3597	572	1361	967	2461	1164	4.10
14	1,286,243	632,669	10.18	12,223	3262	572	1716	1144	4262	1120	7.65
15	1,491,424	926,369	11.25	14,342	3576	573	2089	1331	4516	1170	9.22
16	1,093,644	713,008	12.67	13,745	3950	562	1598	1080	3315	1190	6.85
					Hydrogen						
17	704,310	502,695	3.89	5,864	2048	557	1422	990	2403	1160	4.2
18	1,035,350	714,972	3.86	6,598	2105	560	1790	1175	3231	1185	6.1
19	1,339,878	910,827	3.79	7,253	2134	562	2148	1352	3954	1196	7.75
20	1,621,332	1,047,031	3.74	7,621	2199	562	2386	1474	4351	1244	8.85
21	1,878,363	1,216,896	3.68	8,053	2314	573	2712	1643	4701	1280	10.0
22	1,959,774	1,451,306	6.16	10,846	3571	557	2107	1332	4136	1400	9.25
23	2,417,414	1,728,637	5.82	11,393	3560	565	2492	1529	4749	1440	11.2

TABLE II. - Continued. EXPERIMENTAL RESULTS

(b) Local outside surface temperatures of the test section

Run	Distance from inlet, in.																			
	0	1/16	5/8	1 1/8	1 5/8	2 1/8	2 5/8	3 1/8	3 5/8	4 1/8	4 5/8	5 1/8	5 5/8	6 1/8	6 5/8	7 1/8	7 5/8	8 1/8	8 5/8	8 15/16	9
Hydrogen																					
1	568	630	810	910	[a]1000	[a]1080	[a]1160	[a]1235	[a]1330	[a]1430	[a]1550	[a]1690	[a]1855	[a]2050	2283	2649	3068	3588	3348	1565	600
2	568	630	805	900	[a]950	[a]995	[a]1050	[a]1100	[a]1160	[a]1230	[a]1320	[a]1430	[a]1550	[a]1705	[a]1920	2277	2739	3153	2896	1420	590
3	568	635	825	935	[a]1025	[a]1130	[a]1230	[a]1330	[a]1440	[a]1570	[a]1700	[a]1865	[a]2045	2260	2476	3000	3660	4112	3745	1800	620
4	563	620	805	900	[a]1000	[a]1180	[a]1160	[a]1240	[a]1330	[a]1415	[a]1520	[a]1640	[a]1780	[a]1955	2193	2584	3118	3600	3112	1515	580
5	567	625	810	910	[a]1000	[a]1060	[a]1130	[a]1200	[a]1295	[a]1400	[a]1515	[a]1660	[a]1820	2048	2339	2745	3325	3830	3402	1645	590
6	568	630	820	920	[a]1000	[a]1070	[a]1145	[a]1225	[a]1310	[a]1405	[a]1520	[a]1650	[a]1820	[a]2040	2339	2733	3348	4105	3594	1715	595
7	568	630	830	940	[a]1040	[a]1135	[a]1240	[a]1345	[a]1460	[a]1590	[a]1140	[a]1920	2148	2476	2936	3516	4236	4530	4186	2005	610
8	570	690	1015	1255	[a]1680	2774	3277	3964	4644	4969	5157	5229	5281	5268	[a]5270	5248	5216	5189	4803	2345	660
9	562	610	807	912	[a]1010	[a]1115	[a]1220	[a]1340	[a]1460	[a]1600	[a]1755	[a]1940	2159	2385	2843	3348	3830	4220	3684	1610	590
10	565	625	835	955	[a]1085	[a]1210	[a]1350	[a]1500	[a]1680	[a]1890	[a]2130	2351	2942	3492	4050	4423	4644	4745	4224	1860	610
11	567	640	860	993	[a]1175	[a]1340	[a]1520	[a]1715	[a]1925	2238	2476	2936	3564	4149	4574	4790	4899	4880	4361	1950	620
Helium																					
12	572	610	790	890	[a]995	[a]1080	[a]1160	[a]1250	[a]1360	[a]1480	[a]1630	[a]1800	[a]2005	2294	2843	2456	3989	4217	3360	1400	580
13	572	625	810	920	[a]1005	[a]1080	[a]1170	[a]1310	[a]1500	[a]1730	[a]2220	2407	2936	3564	4236	4764	5021	4989	3977	1625	595
14	577	640	875	1040	2971	3769	4075	4486	4918	5176	5307	5425	5464	5491	5616	5630	5491	5229	4186	1710	610
15	573	810	1645	2520	[a]3600	4224	4701	5008	5099	5202	5202	5268	5307	5372	5386	5399	5386	5281	4536	2040	650
16	562	650	880	1030	[a]1260	[a]1560	[a]1920	[a]2340	2855	3265	3866	4373	4854	5202	5372	5307	5281	4995	4162	1850	620
Hydrogen																					
17	555	605	810	935	[a]1055	[a]1165	[a]1260	[a]1370	[a]1540	[a]1770	2215	2601	3006	3588	4050	4336	4517	[a]4500	3842	1640	590
18	560	630	880	1060	[a]1330	[a]1640	[a]2020	2481	2995	3564	4032	4386	4606	4733	4835	4892	4880	4777	4087	1780	610
19	560	695	1170	1670	[a]2400	3118	3704	4286	4593	4777	4892	4944	4957	4995	5047	5060	5086	5021	4511	1985	630
20	560	770	1580	2405	[a]3460	4124	4643	4828	4969	5066	5073	5125	5099	5131	5176	5248	5307	5255	4841	2195	640
21	570	870	2125	3210	[a]4100	4739	5047	5138	5216	5255	5255	5307	5307	5386	5405	5471	5544	5544	5229	2425	670
22	550	710	1135	1500	[a]2060	3147	3564	4311	4912	5203	5281	5412	5333	5333	5333	5380	5380	5380	5021	2275	655
23	560	810	1760	2770	[a]3920	4765	5176	5294	5405	5445	5412	5438	5386	5412	5491	5570	5623	5623	5333	2550	680

[a]Values taken from faired curves.

TABLE II. - Concluded. EXPERIMENTAL RESULTS

(a) For increments

Increment	Local heat-transfer coefficient, h	Average outside surface temperature of increment, T_s	Average bulk temperature of increment, T_b	Increment	Local heat-transfer coefficient, h	Average outside surface temperature of increment, T_s	Average bulk temperature of increment, T_b
Run 1				Run 4			
1	1077	760	578	1	1115	747	573
2	903	950	602	2	881	940	598
3	848	1090	636	3	808	1090	632
4	803	1235	676	4	773	1235	673
5	771	1410	723	5	753	1395	720
6	741	1635	779	6	731	1585	775
7	719	1930	847	7	718	1845	841
8	692	2370	933	8	690	2276	925
9	649	3080	1045	9	593	3173	1037
10	132	3120	1122	10	191	3049	1120
Run 2				Run 5			
1	1318	742	579	1	1191	760	578
2	936	920	603	2	929	945	603
3	904	1005	634	3	860	1080	637
4	883	1100	669	4	823	1220	677
5	849	1220	708	5	701	1370	723
6	811	1380	754	6	761	1600	778
7	773	1610	808	7	733	1915	846
8	722	2000	878	8	714	2340	932
9	626	2760	972	9	613	3360	1050
10	403	2698	1059	10	247	3267	1144
Run 3				Run 6			
1	1074	769	578	1	1208	747	570
2	925	970	604	2	920	950	596
3	841	1140	640	3	871	1080	631
4	790	1330	684	4	827	1220	671
5	761	1540	736	5	801	1385	719
6	741	1790	799	6	770	1600	774
7	724	2130	877	7	744	1910	843
8	712	2680	978	8	719	2410	932
9	616	3653	1110	9	621	3440	1055
10	124	3573	1199	10	290	3507	1159

TABLE II. - Concluded. EXPERIMENTAL RESULTS

(c) Continued. For increments

Increment	Local heat-transfer coefficient, h	Average outside surface temperature of increment, T_s	Average bulk temperature of increment, T_b
Run 7			
1	1205	756	578
2	917	980	605
3	833	1155	642
4	972	1340	686
5	760	1555	740
6	741	1840	805
7	722	2280	889
8	672	3070	1003
9	591	4200	1155
10	182	3884	1264
Run 8			
1	633	889	581
2	716	1460	624
3	600	2515	715
4	537	4060	865
5	533	4880	1069
6	556	5190	1297
7	587	5275	1532
8	627	5270	1764
9	675	5215	1990
10	-106	4529	2089
Run 9			
1	836	740	571
2	720	960	598
3	655	1135	638
4	616	1330	686
5	591	1565	744
6	576	1865	816
7	563	2265	908
8	536	2905	1027
9	473	3889	1181
10	-82	3556	1255
Run 10			
1	741	791	575
2	741	1020	604
3	666	1240	648
4	623	1500	703
5	596	1845	773
6	580	2310	863
7	572	2990	987
8	512	3900	1146
9	485	4733	1337
10	-124	4000	1419
Run 11			
1	668	787	576
2	699	1070	606
3	619	1375	655
4	581	1715	720
5	569	2130	805
6	564	2760	919
7	499	3800	1073
8	486	4580	1264
9	490	4947	1476
10	-153	4124	1559
Run 12			
1	772	738	581
2	634	940	607
3	599	1090	643
4	565	1250	688
5	538	1455	741
6	520	1730	807
7	507	2151	892
8	441	2950	1006
9	382	4000	1154
10	-135	3356	1215

TABLE II. - Concluded. EXPERIMENTAL RESULTS

(c) Continued. For increments

Increment	Local heat-transfer coefficient, h	Average outside surface temperature of increment, T_s	Average bulk temperature of increment, T_b
	Run 13		
1	603	756	580
2	634	950	605
3	613	1090	643
4	565	1310	692
5	514	1685	756
6	478	2250	845
7	428	3190	970
8	371	4356	1137
9	344	5022	1328
10	-168	3889	1394
	Run 14		
1	330	831	580
2	452	2000	643
3	296	3720	777
4	303	4560	954
5	283	5080	1153
6	273	5380	1353
7	273	5520	1550
8	285	5520	1745
9	286	5556	1936
10	-763	4151	1873
	Run 15		
1	118	1436	581
2	355	3044	659
3	344	4351	827
4	339	5036	1037
5	353	5190	1261
6	375	5245	1490
7	390	5330	1720
8	409	5400	1951
9	437	5370	2180
10	-557	4453	2192

Increment	Local heat-transfer coefficient, h	Average outside surface temperature of increment, T_s	Average bulk temperature of increment, T_b
	Run 16		
1	173	800	565
2	565	1150	591
3	485	1630	648
4	441	2330	734
5	423	3190	857
6	402	4130	1019
7	371	4990	1212
8	366	5431	1421
9	392	5364	1633
10	-412	4036	1669
	Run 17		
1	625	751	567
2	581	985	596
3	553	1165	641
4	542	1390	698
5	513	1730	771
6	462	2400	873
7	429	3200	1014
8	405	4090	1196
9	409	4529	1407
10	-267	3578	1469
	Run 18		
1	419	800	568
2	548	1185	604
3	483	1710	675
4	445	2480	782
5	413	3440	936
6	404	4240	1135
7	416	4655	1362
8	436	4840	1600
9	463	4862	1835
10	-522	3773	1871

TABLE II. - Concluded. EXPERIMENTAL RESULTS

(c) Concluded. For increments

Increment	Local heat-transfer coefficient, h	Average outside surface temperature of increment, T_s	Average bulk temperature of increment, T_b
	Run 19		
1	257	1018	572
2	449	2010	637
3	396	3230	776
4	391	4220	974
5	398	4730	1210
6	421	4910	1461
7	452	4980	1714
8	480	5050	1964
9	515	5070	2208
10	-592	4182	2235
	Run 20		
1	186	1342	575
2	423	2850	670
3	403	4190	870
4	419	4820	1127
5	441	5025	1408
6	469	5110	1689
7	510	5130	1965
8	549	5200	2236
9	579	5285	2501
10	-778	4476	2509
	Run 21		
1	173	1707	591
2	427	3550	718
3	422	4742	972
4	448	5150	1275
5	481	5250	1591
6	523	5300	1902
7	570	5340	2206
8	619	5415	2506
9	653	5560	2803
10	-728	4867	2831

Increment	Local heat-transfer coefficient, h	Average outside surface temperature of increment, T_s	Average bulk temperature of increment, T_b
	Run 22		
1	370	1022	566
2	649	1760	616
3	574	2990	726
4	528	4370	896
5	532	5133	1112
6	554	5391	1350
7	601	5330	1591
8	639	5350	1827
9	675	5390	2058
10	-256	4702	2139
	Run 23		
1	206	1529	576
2	561	3310	673
3	534	4844	878
4	563	5305	1134
5	597	5420	1406
6	642	5420	1678
7	693	5420	1943
8	737	5505	2203
9	777	5610	2461
10	-368	5084	2541

2/17/85

"The National Aeronautics and Space Administration . . . shall . . . provide for the widest practical appropriate dissemination of information concerning its activities and the results thereof . . . objectives being the expansion of human knowledge of phenomena in the atmosphere and space."

—National Aeronautics and Space Act of 1958

NASA SCIENTIFIC AND TECHNICAL PUBLICATIONS

TECHNICAL REPORTS: Scientific and technical information considered important, complete, and a lasting contribution to existing knowledge.

TECHNICAL NOTES: Information less broad in scope but nevertheless of importance as a contribution to existing knowledge.

TECHNICAL MEMORANDUMS: Information receiving limited distribution because of preliminary data, security classification, or other reasons.

CONTRACTOR REPORTS: Technical information generated in connection with a NASA contract or grant and released under NASA auspices.

TECHNICAL TRANSLATIONS: Information published in a foreign language considered to merit NASA distribution in English.

TECHNICAL REPRINTS: Information derived from NASA activities and initially published in the form of journal articles or meeting papers.

SPECIAL PUBLICATIONS: Information derived from or of value to NASA activities but not necessarily reporting the results of individual NASA-programmed scientific efforts. Publications include conference proceedings, monographs, data compilations, handbooks, sourcebooks, and special bibliographies.

Details on the availability of these publications may be obtained from:

SCIENTIFIC AND TECHNICAL INFORMATION DIVISION

NATIONAL AERONAUTICS AND SPACE ADMINISTRATION

Washington, D.C. 20546